JOURNAL OF APPLIED ELECTROCHEMISTRY **27** (1997) 1135–1142

Degradation behaviour of 6013-T6, 2024-T3 alloys and pure aluminium in different aqueous media

P. CARBONINI, T. MONETTA, D. B. MITTON*, F. BELLUCCI‡

Department of Materials and Production Engineering, University of Naples "Federico II", Piazzale Tecchio 80, 80125 Napoli, Italy

P. MASTRONARDI, B. SCATTEIA

Alenia - Un'Azienda Finmeccanica, Piazzale dell'Aeronautica, 80038 Pomigliano, (Na), Italy

Received 3 October 1996; revised 8 November 1996

The electrochemical and corrosion behaviour of 6013-T6, 2024-T3 aluminium alloys and pure aluminium in 0.6 M NaCl and 0.3 M Na_2SO_4 aqueous solutions was investigated using d.c. and a.c. electrochemical techniques. Results show that the 6013-T6 alloy exhibits superior corrosion resistance compared with that exhibited by the 2024-T3 alloy in both environments. These findings were interpreted on the basis of a barrier oxide film model.

1. Introduction

The alloy 6013-T6 offered an improved performance with respect to other Al alloys, such as 2024-T3, 6061-T6 and the 7XXX series high strength alloys, which are currently used in aeronautical applications.

When wedge tested, 6013-T6 exhibits better cracking resistance than 7021-T6 [1, 2]. Compared to 2024-T3, 6013-T6 has a 12% higher tensile strength, 14% lower ultimate strength, 30% higher compression yield strength, similar fracture toughness (which makes it applicable for use in aircraft wing lower surfaces and fuselages, for Mach numbers up to 2), 3% lower density, and a slightly lower cost. The one shortcoming appears to be a 20% lower fatigue performance compared to 2024-T3 in the presence of small surface damage ('nicks' and 'dings') on the edges of otherwise smooth fatigue coupons. When fatigue tested after corrosion of coupons, however, both 2024-T3 and 6013-T6 give similar results [3, 4]. Finally, 6013-T6 is easily weldable, while welding of 2024-T3 requires the use of an inert gas shielded process [5].

Results obtained in the Alcoa laboratories indicate that 6013-T6 has excellent resistance to corrosion and is virtually immune to exfoliation and stress corrosion cracking (SCC) [6, 7]. During outdoor exposure to various environments, 6013-T6 is as resistant to corrosion as 6061-T6. In more corrosive environments (acidified 5% NaCl spray, wet pine wood contact and sea water) 6013-T6 is slightly less resistant than 6061-T6. The corrosion resistance of 6013-T6 is superior to 2XXX and 7XXX series high strength alloys [6, 7].

These properties make 6013-T6 attractive for use in some aircraft parts where other Al alloys, such as 2024-T3, were previously utilized. The main difference between the two alloys is in the Cu content, which is 4.2 wt % in 2024-T3 and only 0.8% in 6013-T6.

This work assesses the electrochemical and corrosion behaviour of 6013-T6, 2024-T3 and pure aluminium (99.99%), in aerated and deaerated 0.6 M aqueous NaCl and 0.3 M Na_2SO_4 at room temperature, by employing both electrochemical (d.c. and a.c.) and weight loss techniques [8]. The d.c. polarization technique, according to Dignam [9], is useful in the study of ionic current in oxide films on aluminium and can supply information about the porous nature of the oxide film [10], the critical pitting potential of aluminium [11], and the corrosion resistance of its oxide layer [12]. The a.c. technique permits the examination of phenomena not clearly detectable with d.c. polarization [8]. Such phenomena include low corrosion rate, ionic sorption or the effect of a corrosion inhibitor on the aluminium oxide layer [13, 14]. Simple models (electrical equivalent circuits) that describe physical phenomena occurring at the aluminium oxide/solution interface [15–17] and/or inside the oxide film [18–20] can be developed. Some authors report information on complex electrochemical reactions occurring at the interface [21–23], even in non-neutral media [24–27]. Electrochemical impedance spectroscopy (EIS) is widely employed even when localized corrosion occurs [28–30] and Mansfeld *et al.* [31, 32] report the appearance of characteristic changes in the impedance spectra when pitting reaches a certain minimum depth.

2. Experimental details

The metallic materials tested in this investigation were aluminium alloys 6013-T6, 2024-T3 and pure

* Permanent address: Massachusetts Institute of Technology, H. H. Uhlig Corrosion Laboratory, Department of Materials Science and Engineering, Cambridge, MA 02139, USA.
‡ To whom correspondence should be addressed.

Table 1. Chemical composition of 2024-T3 and 6013-T6 aluminium alloys

Al alloys	*Cu*	*Mg*	*Si*	*Mn*	*Fe*
2024	4.20	1.60	0.50*	0.30	0.50*
6013	0.80	0.95	0.75	0.35	0.30*

* max

aluminium. The composition of these alloys is presented in Table 1. Dissolution rates in mg dm^{-2} day^{-1} (mdd) of all metallic materials (50 mm × 25 mm × 1 mm specimens) were obtained from weight loss measurements in neutral aerated aqueous 0.6 M NaCl (3.5 wt %), adjusted to pH 7 by using NaOH or HCl with an air flow of approximately 50 or 200 cm^3 min^{-1}. In addition, weight loss measurements were performed in deaerated solutions.

Before each experiment, the surface of the metallic electrode was cleaned with fine emery paper, rinsed in distilled water, degreased in acetone, dried in an air stream and then weighed. After the corrosion test, the specimens were washed in distilled water, deoxidized (10 wt % H_2SO_4 aqueous solution) at room temperature, washed, dried and reweighed. The weight loss due to corrosion was calculated after correction for the weight loss of control specimens in the deoxidizer.

The electrochemical and corrosion behaviour of these materials were studied by exposing specimens to aerated and deaerated neutral aqueous solution of 0.6 M NaCl and 0.3 M Na_2SO_4, respectively. The SO_4^{2-} ion was chosen: (i) to investigate the dielectric properties of the oxide layer [33–36] and (ii) to promote selective attack of the Cu on the exposed surface of the Al alloys.

To perform polarization and impedance measurement, specimens of 6013-T6, 2024-T3 and pure aluminium of about 1 cm^2 surface area were cleaned with emery paper (to 0000 grit), polished to a mirror finish (0.3 μm Al_2O_3 suspension), rinsed with distilled water and stored in a desiccator until the beginning of the test. Potentiodynamic polarization curves and EIS measurements were carried out in a conventional three electrode electrochemical cell, with a platinum counter electrode and a reference electrode placed in a Luggin capillary with the tip located approximately 1 or 2 mm from the specimen surface. Either a saturated calomel (SCE) or saturated sulfate (SSE) electrode (when testing Al alloys in Na_2SO_4) was used for the reference. Unless otherwise indicated, all potentials are referred to a SCE electrode. Before each experiment, the working electrode was left at open circuit for about 2 h to reach a stable corrosion potential. The solution was mechanically stirred and either aerated or purged with argon, in accordance with the procedure followed by others [18, 19, 33, 37–40].

Potentiodynamic polarization curves were recorded at a scan rate of 30 mV min^{-1} using an EG&G PAR 273 potentiostat controlled by an Olivetti M290S computer using PARCALC^{TM} software. Potentiodynamic polarization experiments were carried out in a single sweep starting from 200 to 500 mV below the corrosion potential and ending about 100 mV above the pitting potential, when the pitting potential was observed.

Electrochemical impedance spectroscopy was performed at the corrosion potential using a Schlumberger Solartron 1255 frequency response analyser connected to an EG&G PAR 273 potentiostat. The analyser was controlled by an Olivetti M290S computer using a software program described in the literature [41, 42]. In general the frequency was monitored between 10^5 and 10^{-2} Hz at ten points per decade. The amplitude of the superimposed potential was 10 mV with respect to E_{corr}. High frequency shift errors due to the use of the EG&G PAR 273 [43] were numerically corrected.

3. Results and discussion

3.1. *Weight loss analysis*

The corrosion of pure aluminium and the two alloys (6013-T6, 2024-T3) was evaluated in 0.6 M NaCl in the presence and absence of an air stream. Figure 1(a) presents the weight loss per unit area as a function of time at 25 °C in the presence of an air flow of

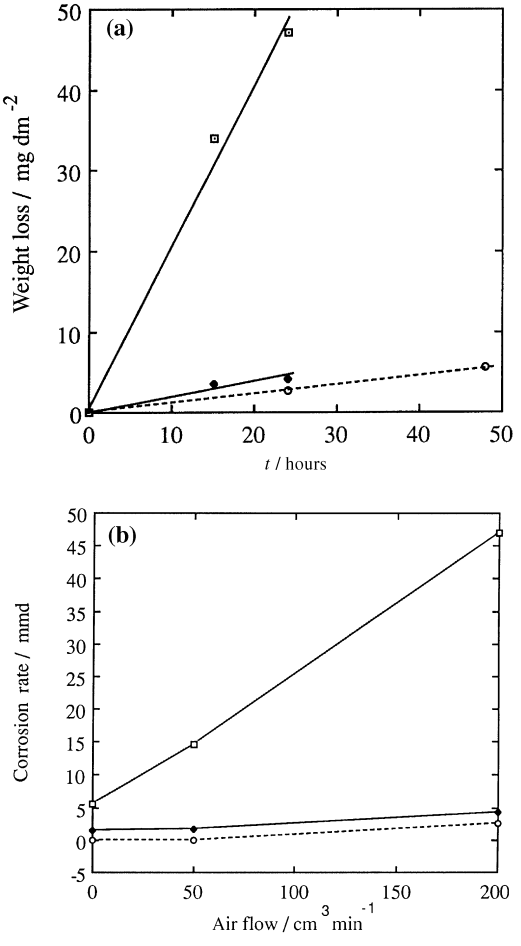

Fig. 1. (a) Weight loss in mg dm^{-2} as a function of time at an air flow of 200 cm^3 min^{-1}, and (b) corrosion rate as a function of air flow for the 2024-T3 (□), 6013-T6 (♦) and pure aluminium (○) in a 0.6 M neutral air saturated aqueous solution of NaCl at 25 °C.

$200\,cm^3\,min^{-1}$. Figure 1(b) presents the corrosion rate for the same materials as a function of the amount of air flow.

It is apparent from Fig. 1(a) that in the presence of an air flow of $200\,cm^3\,min^{-1}$ the alloy 2024-T3 suffers significantly more corrosion than either of the other materials. Further, pure aluminium and the alloy 6013-T6 exhibit similar weight loss data. The data presented in Fig. 1(b) reveal that the dissolution of Al and both of the alloys is influenced by the change in the level of oxygen in the solution. However, the corrosion rate of 2024-T3 increases much more rapidly with increasing air flow than either of the other materials. In addition, the corrosion rate of 6013-T6 and pure aluminium parallel each other with the alloy exhibiting slightly higher dissolution for all flow rates. These data suggest that, for the conditions studied, the air formed film developed on 6013-T6 exhibits protective properties similar to that of pure aluminium and significantly better than that formed on the 2024-T3 alloy. In addition, these data suggest that the diffusion of cathodic reactant (oxygen) to the metallic surface is the rate limiting process. This result is in agreement with those reported in the literature [37, 39, 44].

3.2. *Electrochemical experiments: d.c. techniques*

It should be noted that while aluminium and its oxide layer are susceptible to Cl^- ions, they are almost immune to SO_4^{2-} ions [34]. This is a useful characteristic for investigating the electrochemical properties of aluminium and its alloys. The SO_4^{2-} ion is aggressive to Cu even in the absence of Cl^-[34], thus, Al alloys with a high percentage of copper (such as 2024-T3) may, in an aerated environment, suffer from pitting corrosion due to the presence of SO_4^{2-}.

The potentiodynamic polarization curves for pure Al and the two alloys tested (2024-T3 and 6013-T6) are reported in Fig. 2 for Na_2SO_4 and in Fig. 3 for NaCl.

In the deaerated Na_2SO_4 solution (Fig. 2(a)), the cathodic reaction is assumed to be the evolution of hydrogen. Although 6013-T6 exhibits a more active E_{corr} value, the anodic polarization curves for pure aluminium and this alloy exhibit the same general features. Thus there is no active–passive transition and the passive current densities for the two materials are virtually the same. These features are indicative of a material which has formed a protective passive film prior to initiation of the experiment. This is not surprising as Al_2O_3 is thermodynamically possible at potentials well below the open circuit potential (o.c.p.) recorded during this experiment. In this environment the polarization curves are not smooth in the passive region, which has been interpreted by Moshier *et al.* [33] in terms of a surface instability due to clustering of SO_4^{2-} ions inside the film. The 2024-T3 alloy exhibits similar behaviour to the other materials except for an anodic peak which transverses the potential range between approximately −0.200

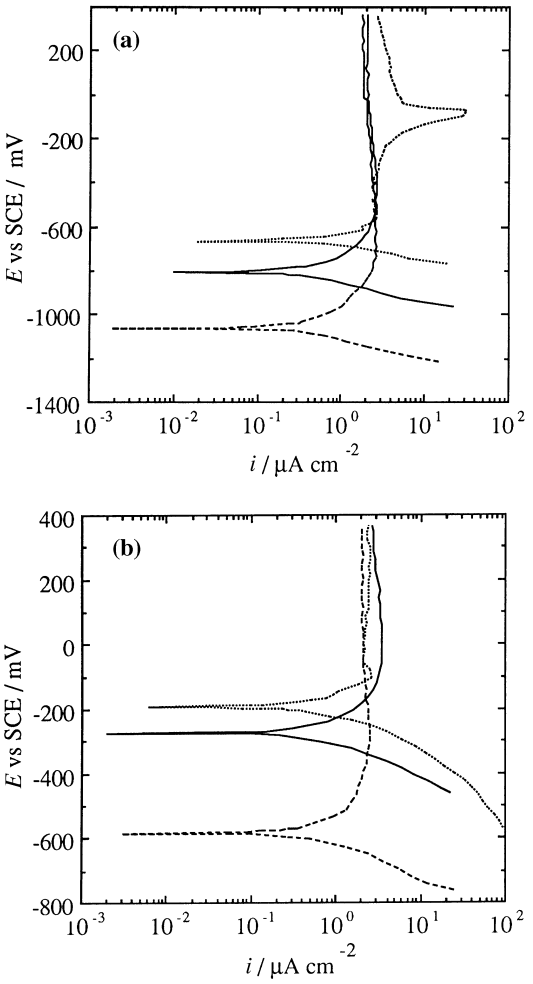

Fig. 2. Potentiostatic polarization curves for the aluminium alloys 2024-T3 (·····), 6013-T6 (——) and pure aluminium (– – – –) in neutral deaerated (a) and aerated (b) 0.3 M Na_2SO_4 at 25 °C.

and −0.050, and exhibits a maxima at about −0.080 V. This is assumed to result from the higher copper content of this alloy and the potential corresponds quite well to the potential associated with the oxidation of Cu to Cu_2O [45].

The potentiodynamic curves for pure aluminium and the alloys 6013-T6, 2024-T3 Al in an aerated Na_2SO_4 solution are presented in Fig. 2(b). Again the three curves exhibit similar general features, with aluminium displaying the lowest passive current density. The 2024-T3 curve reveals a small anodic peak with a maxima at a potential (−0.105 V) within 25 mV of that recorded for the same alloy in the deaerated solution (Fig. 2(a)). In addition, while the passive current density for the 6013-T3 initially exhibits the highest value, it decreases with increasing applied potential. Conversely, over the same potential range, the passive current density for the 2024-T3 alloy revealed an increase.

Figure 3(a) presents the behaviour, in deaerated 0.6 M NaCl, for pure Al and the two alloys being evaluated. In this electrolyte, pure Al exhibits passive behaviour in the potential range −1100 to −780 mV. It is believed that, in this passive potential region, adsorption of Cl^- at the oxide film/solution interface

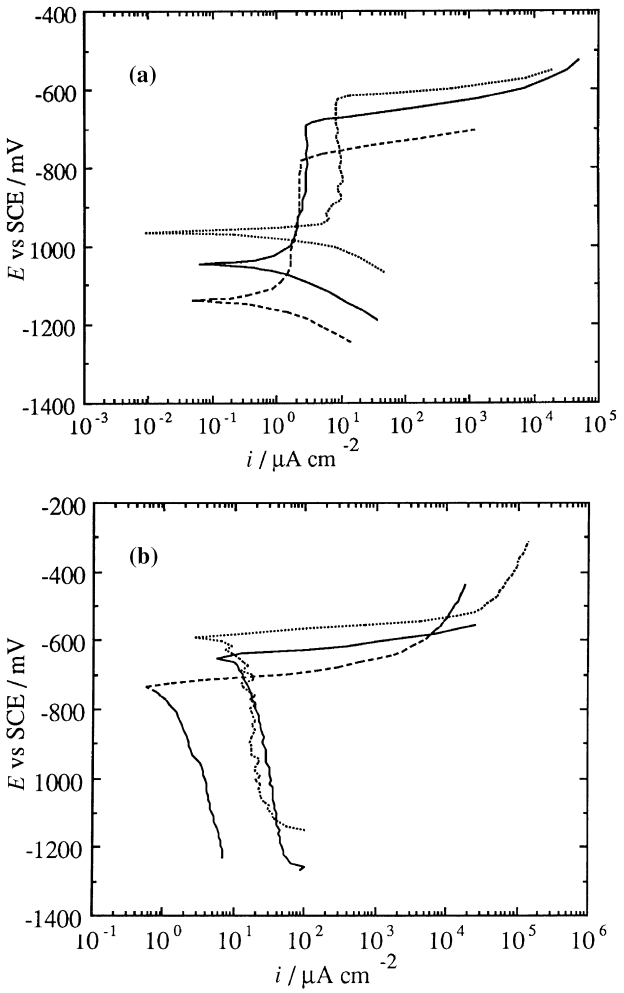

Fig. 3. Potentiostatic polarization curves for the aluminium alloys 2024-T3 (· · · · · ·), 6013-T6 (——) and pure aluminium (– – – –) in neutral deaerated (a) and aerated (b) 0.6 M NaCl at 25 °C.

leads to an increase in the rate of metastable pit nucleation [46]. The adsorption of Cl^- increases with applied potential up to the pitting potential, E_p, at which time a transition from metastable to stable pit growth occurs and a sharp rise in anodic current is observed. These phenomena are consistent with the conclusions reported by Pride, Scully and Hudson [46] and Beccaria and Poggi [47]. The behaviour of 6013-T6 and 2024-T3 is qualitatively close to that of pure Al. Passive behaviour is observed in the potential range from −1050 to −650 mV for the 6013-T6, and in the potential range from −960 to −595 mV for the 2024-T3 alloy. Although the pitting potential increases in the order Al < 6013-T6 < 2024-T3, the passive current density is significantly higher for the 2024-T3 alloy than for the other two materials, which display similar values.

The following parameters can be utilized to rank alloy susceptibility to pitting: (i) the pitting potential, E_p, (ii) the values of current and anodic slope at this potential, and (iii) the polarization resistance, R_p calculated through a linear regression of the data recorded in an interval of ±10 mV around E_{corr} [39]. These values are reported in Table 2. By using Faraday's law the current at $E = E_p$ can be converted to mdd. Values obtained are 9.17, 0.764 and 0.20 mdd for the 2024-T3, 6013-T6, and pure aluminium, respectively. These values provide a ranking of the corrosion rate which is analogous to that determined for the weight loss data.

Table 2. Pitting potential, E_p (mV vs SCE), current density, $i(\mu A\,cm^{-2})$, anodic Tafel slope, b_a ($mV\ dec^{-1}$), and polarization resistance, R_p ($k\Omega cm^2$) for 2024-T3, 6013-T6 Al alloys and pure Al, in 0.6 M NaCl deaerated neutral aqueous solution

Alloy	E_p /mV	*i at* $E=E_p$ /μA cm^{-2}	b_a at $E=E_p$ /mV dec^{-1}	R_p /kΩ cm^2
2024-T3	−590	10	18.7	0.46
6013-T6	−650	0.9	23.2	20.8
Pure Al	−738	0.25	15.5	145

Figure 3(b) presents the potentiodynamic polarization curves, in aerated 0.6 M NaCl, for the materials under investigation. None of the three materials exhibit any passive behaviour. The values of the corrosion potentials for 2024-T3, 6013-T6 and pure aluminium are −0.600, −0.652 and −0.750, respectively. In each case this value is within a few millivolt of the pitting potential determined in the analogous deaerated solution. This result supports the view that corrosion of these alloys in aerated NaCl progresses by pitting. In addition, it has been observed that E_{corr} of each material has shifted in the noble direction with respect to that recorded in the deaerated electrolyte and the cathodic branch of the polarization curves display diffusion control. The latter observation is in agreement with the results of Bellucci [37], Berrada *et al.* [39] and Mansfeld *et al.* [44]. It is also apparent from this figure that the cathodic behaviour of 6013-T6 is quite similar to that of 2024-T3, while significantly lower cathodic currents were observed on pure Al. It is assumed that the higher cathodic current density for the alloys results from the presence of copper at the surface. The latter provides a good site for the cathodic reaction. That the two alloys display quantitatively similar cathodic curves suggests that the solution transport properties of oxygen and not the level of Cu in the alloy is rate limiting. A visual inspection of the specimens provided the following ranking in order of decreasing susceptibility to pitting corrosion: 2024-T3 > 6013-T6 > pure Al.

3.3. *Electrochemical impedance spectroscopy*

Although d.c. measurements provide information about electrode kinetics for processes occurring at potentials far from the open circuit potential EIS is frequently obtained at o.c.p. [18] and this has been followed during the current study.

Interpretation of the results is not simple, because of the complexity of the phenomena occurring for an aluminium oxide layer. Equivalent electrical circuits with constant phase elements (CPEs) have been proposed to interpret experimental data [18, 48–51]. However, according to the current literature on alu-

minium oxide films [19, 36, 38], the best equivalent circuit for modelling phenomena occurring at the oxide/environment interface is presented in Fig.4. A physical description of this model consists of a barrier-type layer covering the aluminium substrate. The electrical properties of this layer affect the corrosion characteristics of the metallic substrate. The equivalent circuit represented in Fig. 4 incorporates three time constants related to the structure and properties of this layer (R_p and (C_p) and to the dynamics of the electrochemical interfacial reaction (L, R_L, C_{dl} and R_{ct}). This model has been proposed to simulate the behaviour of oxide films formed on pure aluminium in different aqueous media (0.5 M NaCl and Na_2SO_4) [19]. In subsequent sections, however, this model has also been adopted for interpretation of the data from the aluminium alloys investigated during this study.

Figure 5 presents a.c. spectra for the three materials being investigated in deaerated Na_2SO_4. From the Bode diagram (Figure 5(a)) we observe that 6013-T6, and pure Al exhibit similar behaviour, which is comparable to a single RC circuit over a wide frequency range ($10^{-2} \sim 10^5$ Hz). The second and third time constant as reported in Fig. 4 are currently observed at frequencies below 10^{-2}Hz [19], which is lower than the minimum frequency monitored during the current study. Results shown in Fig. 5 reveal similar capacitive behaviour over the frequency range ($10^0 \sim 10^3$ Hz) for 6013-T6, 2024-T3 and pure aluminium. However, 2024-T3 shows a slightly lower impedance (higher capacitance) at high frequencies. The capacitance is related to the dielectric properties of the film through the expression:

$$C = \varepsilon\varepsilon_0 A l^{-1} \quad (1)$$

where A represents the surface area of the sample, l is the film thickness, C is capacitance, and ε and ε_0 are the dielectric constant and permittivity of a vacuum (8.854×10^{-14} F cm^{-1}), respectively. The higher capacitance observed for the 2024-T3 alloy suggests that the dielectric properties of the protective film are inferior to those of the other two materials.

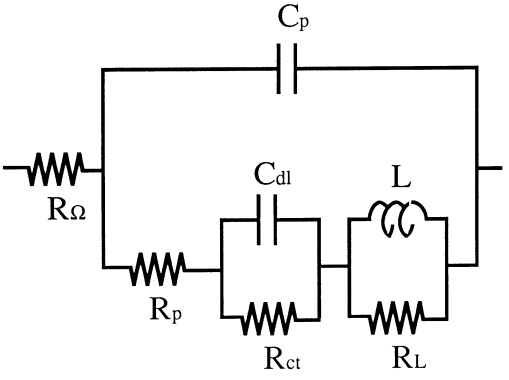

Fig. 4. Equivalent circuit modelling the behaviour of the complex phenomena occurring at the oxide/environment interface when inductive loops are observed.

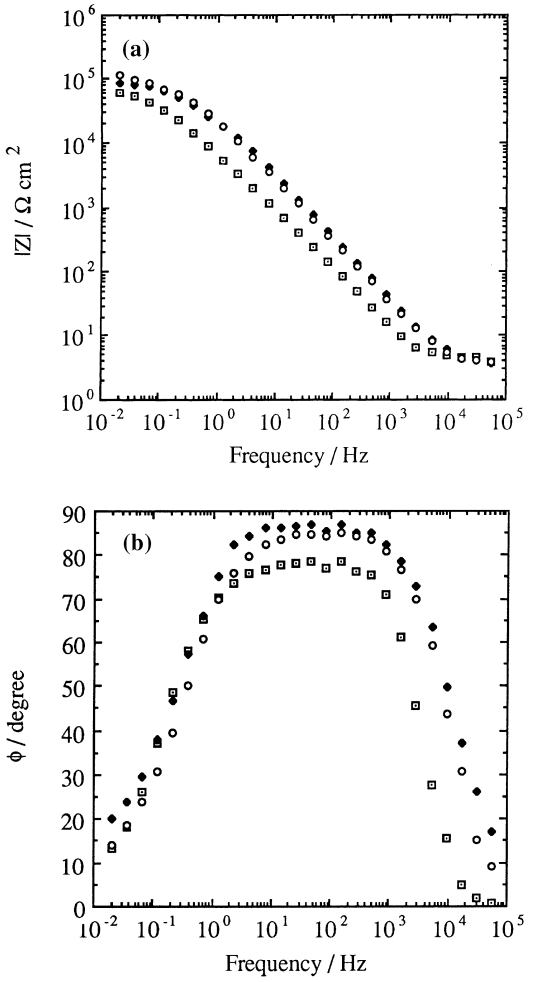

Fig. 5. (a) Impedance modulus and (b) phase angle obtained for 2024-T3 (⊡), 6013-T6 (♦) and pure aluminium (○) in deaerated 0.3 M Na_2SO_4.

Additionally, from Fig. 5(a) it appears that at very low frequencies the impedance is lower for 2024-T3 than for 6013-T6 or pure Al. These two properties (high capacitance at high frequencies and low impedance at low frequencies) exhibited by the 2024-T3 alloy suggest that the protective properties of the film are inferior to those exhibited by the other two materials. The low impedance value observed for the 2024-T3 alloy is indicative of a higher corrosion rate in this environment.

Figures 6(a) and (b) present the results obtained in an aerated neutral aqueous solution of 0.3 M Na_2SO_4. It is obvious from Figure 6(a), that the impedance of pure Al is greater than that revealed by either 2024-T3 or 6013-T6 and this becomes more pronounced with decreasing frequency. The frequency range over which the materials display capacitive behaviour is similar for the three materials and is in the range $10^1 - 10^3$ Hz (Fig. 6(b)). By comparing the data from the aerated (Fig. 6) and deaerated (Fig. 5) Na_2SO_4 solutions it can be seen that the range of capacitive behaviour is narrower in the aerated solution. The narrower frequency range observed suggests that the oxide formed in the aerated solution is less protective than that formed in the deaerated so-

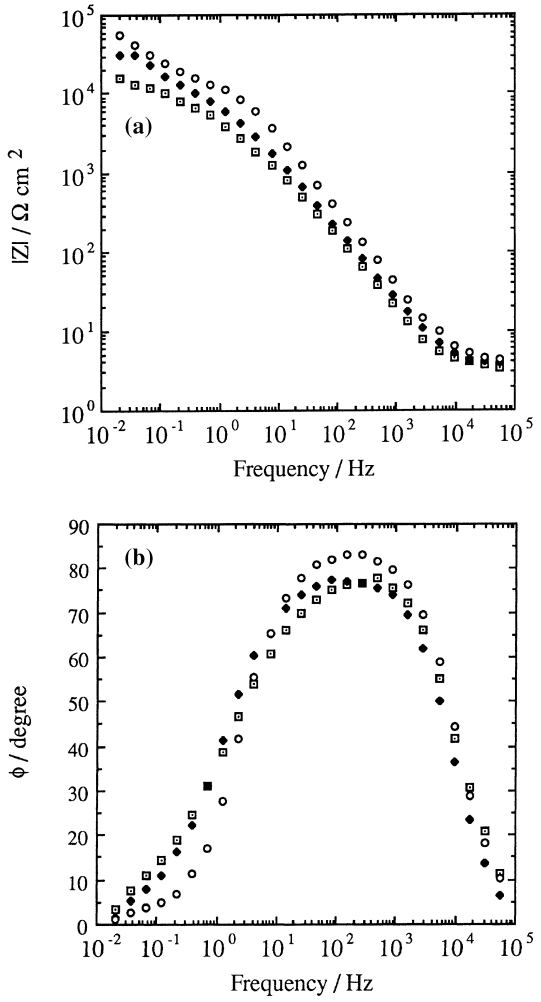

Fig. 6. (a) Impedance modulus and (b) phase angle obtained for 2024-T3 (⊡), 6013-T6 (♦) and pure aluminium (○) in aerated 0.3 M Na_2SO_4.

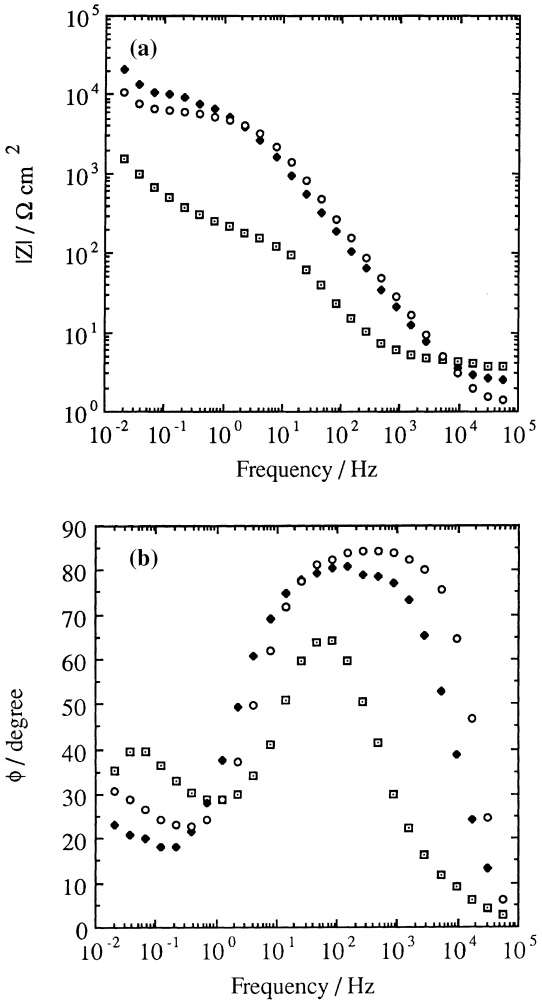

Fig. 7. (a) Impedance modulus and (b) phase angle for 2024-T3 (⊡), 6013-T6 (♦) and pure aluminium (○) in deaerated 0.6 M NaCl.

lution. Furthermore, results at low frequencies show impedance values in the following order pure aluminium > 6013-T6 > 2024-T3. This finding suggests that the superior properties of 6013-T6 arise from an oxide which exhibits a higher impedance than that formed on the 2024-T3. From the low frequency branch of the Bode plot, a second time constant related to the R_{ct} and C_{dl} is observed.

Results obtained in deaerated and aerated 0.6 M NaCl neutral aqueous solutions are reported in Fig. 7 and 8, respectively. In the deaerated solution, the Bode diagram (Figure 7(a)), reveals a similar response over the frequency range $10^0 - 10^4$ Hz for both 6013-T6 and pure Al. Conversely, the low impedance values observed for 2024-T3 suggest that the oxide film is much less resistant than that of the other two materials. In addition, the maximum phase angle value exhibited by 2024-T3 ($\approx 60°$) is much lower than that exhibited by the 6013-T6 ($\approx 80°$) and pure aluminium ($\approx 85°$) (see Figure 7 (b)). Finally, a second time constant is clearly seen in Figs 7(a) and (b). It is worth pointing out that the frequency at which the second time constant appears is higher for the 2024-T3 alloy. This result is consistent with the inferior protective properties of the oxide layer on this alloy [19].

In the aerated 0.6 M NaCl neutral aqueous solution, negative impedance values, or inductive loops, were clearly observed for all the investigated materials (Fig. 8). Thus all three time constants of the equivalent circuit reported in Fig. 4 are apparent. The negative impedance values were reported by numerous authors researching aluminium and have been attributed to adsorption phenomena occurring in the aluminium oxide layer [29, 30, 52–54] or to pitting phenomena observed, at short exposure times, when the values of E_{corr} and E_p are similar [55]. During the current study, an inductive loop was not observed after prolonged immersion in aerated NaCl in agreement with data reported by Mansfeld [55] obtained with 7075-T6 aluminium alloy exposed to 0.5 M NaCl for three days. These results are reported in Fig. 9 for 6013-T6 alloy after 0, 1 and 4 days of immersion in aerated NaCl. Similar results were obtained for the other materials; however, these have been omitted here for the sake of simplicity.

The time required for the inductive loop to disappear is equal to 10 h, 4 and 5 days for the 2024-T3, 6013-T6 and pure aluminium, respectively. Following a model on the pitting of aluminium reported in the literature [19], this time is the time required to reach a

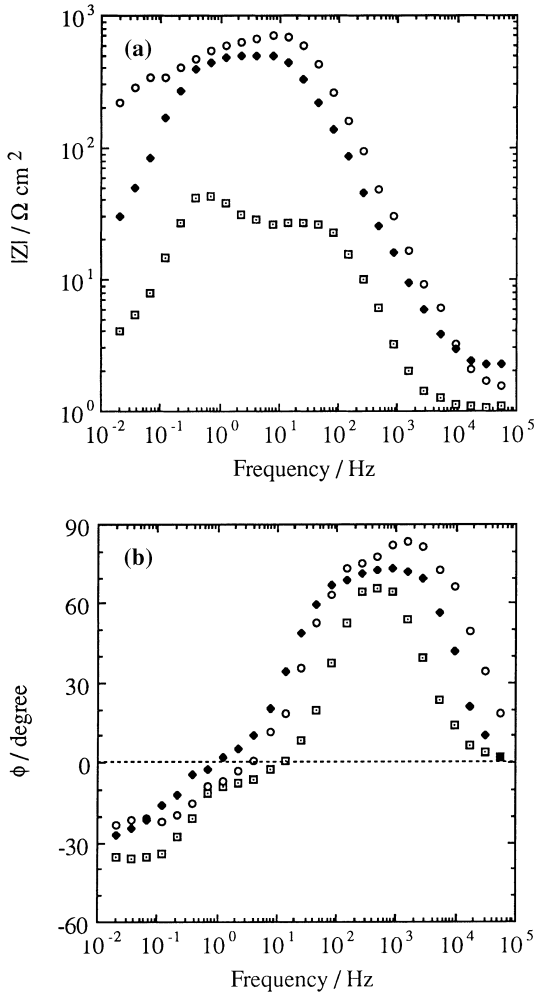

Fig. 8. (a) Impedance modulus, and (b) phase angle for 2024-T3 (⊡), 6013-T6 (♦) and pure aluminium (○) in aerated 0.6 M NaCl upon immersion in the test solution.

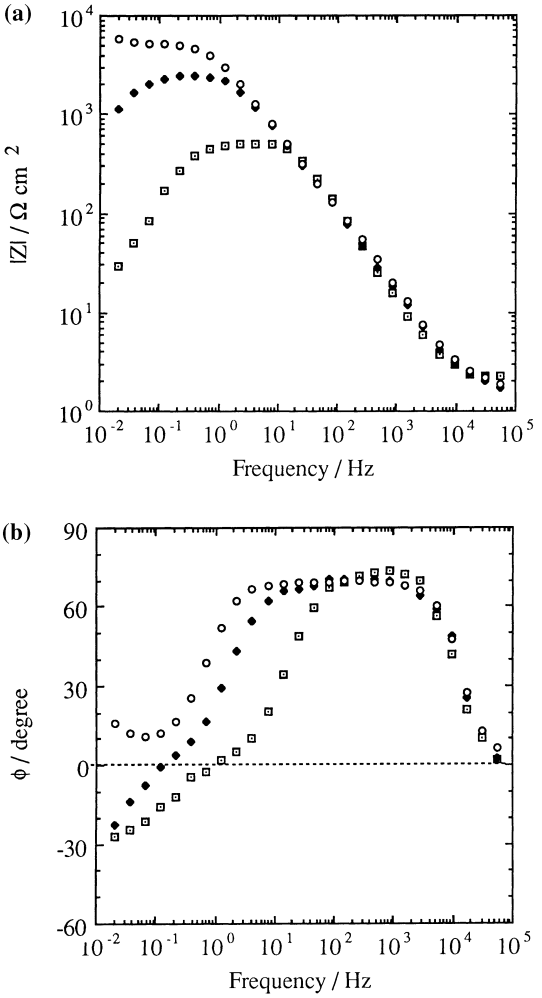

Fig. 9. (a) Impedance modulus and (b) phase angle for 6013-T6 in aerated 0.6 M NaCl after 0 (⊡), 1 (♦) and 4 (○) days immersion in the test solution.

reproducible stationary state in which no intact passive surface area exists. Thus, on this basis, the more resistant an alloy is, the longer it will take for the inductive loop to disappear, suggesting again the protective behaviour in the order: pure aluminium > 6013-T6 > 2024-T3.

4. Conclusions

Results reported in this investigation reveal the superior corrosion resistance of 6013-T6 alloy with respect to the 2024-T3 in aggressive (NaCl) and non aggressive (Na_2SO_4) media. Assuming the presence of an air formed protective oxide on each of the alloys, EIS results suggest that the superior properties of the 6013-T6 alloy are due to a more homogeneous protective oxide layer.

Acknowledgements

The Authors wish to thank Alenia–Un'Azienda Finmeccanica for its financial and technical support of this research. One of the authors (D. B. M.) wishes to acknowledge financial support from the University of Naples Federico II.

References

[1] The Aluminium Association, 818 Connecticut Avenue, NW, Washington, DC 20036, *Aluminium Standard and Data* (1984).
[2] Department of Defense, United States of America, 'Military Standardization Handbook Metallic Materials and Elements for Aerospace Vehicles Structures', June 1 (1987).
[3] M. V. Hyatt and S. E. Axter, 'Aluminium Alloy Development for Subsonic and Supersonic Aircraft', Boeing Commercial Airplane Group, Seattle, Washington (1991).
[4] R. C. Malcolm, Alloy Technology Division, Alcoa Laboratories, 'Fatigue Characterization of Aluminium Alloy X6013-T6 Sheet' 5 Aug. (1985).
[5] R. B. Ross, *in* 'Metallic Material Specification Handbook', 4th edn, Chapman & Hall, New York (1992).
[6] A. J. Becker and J. E. Hall, Alloy Technology Division, Alcoa Laboratories, 'X6013-T6 for General Structural Application, Resistance to Corrosion of Sheet, Plate, and Extrusions' (1985).
[7] A. J. Becker and J. E. Hall, Alloy Technology Division, Alcoa Laboratories, 'X6013-T6 for General Structural Application, Resistance to Stress-Corrosion Cracking of Welded X6013-T6 Plate and Extrusions' (1985).
[8] D. C. Silverman, *Electrochim. Acta* **38** (1993) 2075.
[9] M. J. Dignam, *J. Electrochem. Soc.* **109** (1962) 184.

[10] C. G. Dunn, *ibid.* **115** (1968) 219.
[11] K. Nisancioglu and H. Holtan, *Corros. Sci.* **18** (1978) 835.
[12] S. Sato, Y. Itoi and A. Hasumi, *Electrochim. Acta* **26** (1981) 1303.
[13] C. M. A. Brett, I. A. R. Gomes and J. P. S. Martins, *J. Appl. Electrochem.* **24** (1994) 1158.
[14] F. Mansfeld, *Electrochim. Acta* **35** (1990) 1533.
[15] C. A. Gervasi and J. R. Vilche, *ibid.* **37** (1992) 1389.
[16] H. J. de Wit, C. Wijenberg and C. Crevecoeur, *J. Electrochem. Soc.* **126** (1979) 779.
[17] J. Bessone, C. Mayer, K. Jüttner and W. L. Lorenz, *Electrochim. Acta* **28** (1983) 171.
[18] H. J. W. Lenderink, M. van der Linden and J. H. W. De Wit, *ibid.* **38** (1993) 1989.
[19] J. B. Bessone, D. R. Salinas, C. E. Mayer, M. Ebert and W. J. Lorenz, *ibid.* **37** (1992) 2283.
[20] S. M. Lee and S. I. Pyun, *J. Appl. Electrochem.* **22** (1992) 151.
[21] D. D. Macdonald, *Electrochim. Acta* **35** (1990) 1509.
[22] R. D. Armstrong and M. Henderson, *J. Electroanal. Chem.* **39** (1972) 81.
[23] L. Bai and B. E. Conway, *Electrochim. Acta* **38** (1993) 1803.
[24] C. M. A. Brett, *J. Appl. Electrochem.* **20** (1990) 1000.
[25] D. D. Macdonald, S. Real, S. I. Smedley and M. Urquidi-Macdonald, *J. Electrochem. Soc.* **135** (1988) 2410.
[26] B. van der Linden, H. Terryn and J. Vereecken, *J. Appl. Electrochem.* **20** (1990) 798.
[27] O. R. Brown and J. S. Whitley, *Electrochim. Acta* **32** (1987) 545.
[28] R. Oltra and M. Keddam, *ibid.* **35** (1990) 1619.
[29] F. Mansfeld and M. W. Kendig, *J. Electrochem. Soc.* **135** (1988) 828.
[30] S. E. Frers, M. M. Stefenel, C. Mayer and T. Chierche, *J. Appl. Electrochem.* **20** (1990) 996.
[31] F. Mansfeld and H. Shih, *J. Electrochem. Soc*. **135** (1988) 1171.
[32] F. Mansfeld, S. Lin, S. Kim and H. Shih, *Corros. Sci.* **27** (1987) 997.
[33] W. C. Moshier, G. D. Davis and J. S. Ahearn, *ibid.* **27** (1987) 785.
[34] M. Elboujdaini, E. Ghali, R. G. Barradas and M. Girgis, *ibid.* **30** (1990) 885.
[35] A. Frichet, P. Gimenez and M. Keddam, *Electrochim. Acta* **38** (1993) 1957.
[36] J. De Laet, J. Scheers, H. Terryn and J. Vereecken, *Electrochim. Acta* **38** (1993) 2103.
[37] F. Bellucci, *Corrosion* **17** (1991) 808.
[38] W. J. Lorenz and F. Mansfeld, *Corros. Sci.* **21** (1981) 647.
[39] S. Berrada, M. Elboujdaini and E. Ghali, *J. Appl. Electrochem.* **22** (1992) 1065.
[40] D. C. Silverman, J. E. Carrico, *Corrosion* **36** (1981) 301.
[41] G. Chiodelli, EIS data acquisition program (1991–1994).
[42] G. Chiodelli, P. Lupotto, *J. Electrochem. Soc.* **138** (1991) 2703.
[43] F. Mansfeld, S. Lin, Y. C. Chen and H. Shih, *J. Electrochem. Soc.* **135** (1988) 906.
[44] F. Mansfeld, M. W. Kendig and S. Tsai, *Corrosion* **38** (1982) 570.
[45] M. Pourbaix, in 'Atlas of Electrochemical Equilibria in Aqueous Solutions', Pergamon Press, New York (1966).
[46] S. T. Pride, J. R. Scully and J. L. Hudson, *J. Electrochem. Soc.* **141** (1994) 3028.
[47] A. Beccaria and G. Poggi, *Corrosion* **42** (1986) 470.
[48] B. Boukamp, *in* 'Equivalent Circuit User Manual', University of Twente (1989).
[49] B. Aurian-Blajeni, *J. Appl. Electrochem.* **22** (1992) 553.
[50] F. Mansfeld, *Corrosion* **36** (1981) 301.
[51] P. Kurzweil, J. Ober and D. W. Webner, *Electrochim. Acta* **34** (1989) 1179.
[52] K. Jüttner, *ibid.* **35** (1990) 1501.
[53] F. Mansfeld, Y. Wang and H. Shih, *ibid.* **37** (1992) 2277.
[54] F. Mansfeld, S. Lin, S. Kim and H. Shih, *ibid.* **34** (1989) 1123.
[55] F. Mansfeld, *ibid.* **38** (1993) 1891.